Amino methoxy difluoroboron diketonate as a multicolor and multi-responsive polymorphic fluorescence emitter

Shiho Katsumi, Marine Louis, Tsumoru Morimoto, Chigusa Goto, Shouhei Katao, Fuyuki Ito, Rémi Métivier, Tsuyoshi Kawai, Clémence Allain

▶ **To cite this version:**

Shiho Katsumi, Marine Louis, Tsumoru Morimoto, Chigusa Goto, Shouhei Katao, et al.. Amino methoxy difluoroboron diketonate as a multicolor and multi-responsive polymorphic fluorescence emitter. Journal of Photochemistry and Photobiology A: Chemistry, 2024, 447, pp.115254. ⟨10.1016/j.jphotochem.2023.115254⟩. ⟨hal-04326463⟩

HAL Id: hal-04326463

https://hal.science/hal-04326463v1

Submitted on 6 Dec 2023

HAL is a multi-disciplinary open access archive for the deposit and dissemination of scientific research documents, whether they are published or not. The documents may come from teaching and research institutions in France or abroad, or from public or private research centers.

L'archive ouverte pluridisciplinaire **HAL**, est destinée au dépôt et à la diffusion de documents scientifiques de niveau recherche, publiés ou non, émanant des établissements d'enseignement et de recherche français ou étrangers, des laboratoires publics ou privés.

HAL Authorization

Journal Pre-proofs

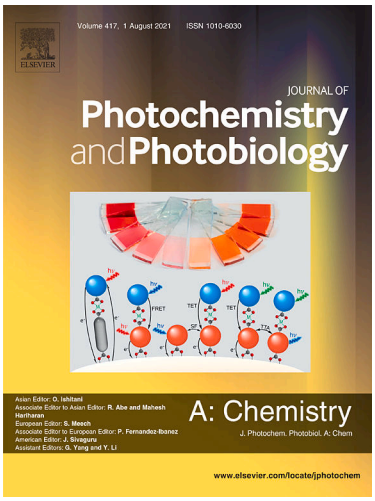

Amino methoxy difluoroboron diketonate as a multicolor and multi-responsive polymorphic fluorescence emitter

Shiho Katsumi, Marine Louis, Tsumoru Morimoto, Chigusa Goto, Shouhei Katao, Fuyuki Ito, Rémi Métivier, Tsuyoshi Kawai, Clémence Allain

PII: S1010-6030(23)00719-0
DOI: https://doi.org/10.1016/j.jphotochem.2023.115254
Reference: JPC 115254

To appear in: *Journal of Photochemistry & Photobiology, A: Chemistry*

Received Date: 9 August 2023
Revised Date: 24 September 2023
Accepted Date: 9 October 2023

Please cite this article as: S. Katsumi, M. Louis, T. Morimoto, C. Goto, S. Katao, F. Ito, R. Métivier, T. Kawai, C. Allain, Amino methoxy difluoroboron diketonate as a multicolor and multi-responsive polymorphic fluorescence emitter, *Journal of Photochemistry & Photobiology, A: Chemistry* (2023), doi: https://doi.org/10.1016/j.jphotochem.2023.115254

This is a PDF file of an article that has undergone enhancements after acceptance, such as the addition of a cover page and metadata, and formatting for readability, but it is not yet the definitive version of record. This version will undergo additional copyediting, typesetting and review before it is published in its final form, but we are providing this version to give early visibility of the article. Please note that, during the production process, errors may be discovered which could affect the content, and all legal disclaimers that apply to the journal pertain.

© 2023 Published by Elsevier B.V.

Journal Pre-proofs

Amino Methoxy Difluoroboron Diketonate as a Multicolor and Multi-Responsive Polymorphic Fluorescence Emitter

Shiho Katsumi[*, **], Marine Louis*, Tsumoru Morimoto*, Chigusa Goto*, Shouhei Katao*, Fuyuki Ito*, Rémi Métivier**, Tsuyoshi Kawai*, Clémence Allain****

* Graduate School of Science and Technology, Nara Institute of Science and Technology, NAIST, Takayama 8916-5, Ikoma, Nara 630-0192, Japan

** Université Paris-Saclay ENS Paris-Saclay, CNRS, PPSM, 91190 Gif-sur-Yvette, France

*** Department of Chemistry, Institute of Education, Shinshu University, 6-Ro, Nishinagano, Nagano 380-8544, Japan

Keywords: fluorescence, difluoroboron diketonate, mechanofluorochromism, acid-base response

Abstract

We here report synthesis and stimuli-responsive fluorescence nature of amino-methoxy-difluoroboron diketonate, **DFB-NH_2**, which was successively prepared via the Curtius rearrangement to introduce a primary amine on the phenyl ring. Thanks to the NH_2 group, the molecule exhibits intermolecular charge transfer (ICT) nature in the ground state of the solution and crystalline phases. We observed a quinoid-like structure and a typical head-to-tail H-type dimer structure in the crystal state. The single crystal with dark-red weak emission demonstrates a blue-shifted emission after mechanical smearing, as a unique mechanofluorochromism (MFC). The drop-casted sample on a paper sheet also demonstrates further significant MFC. Additionally, characteristic acid-/base-responsivity is observed in both the solution phase, polymer-dispersed films, and powder samples.

Journal Pre-proofs

Journal Pre-proofs

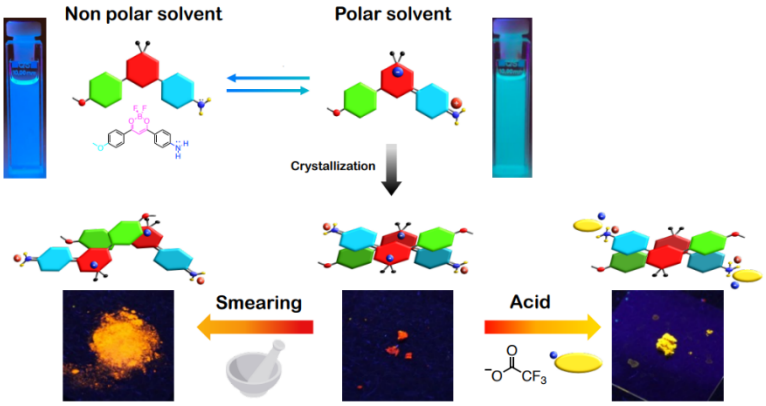

Journal Pre-proofs

Journal Pre-proofs

1. Introduction

Development of new luminescent molecular materials has been of central importance in functional organic chemistry [1–3] for their use in future application fields such as light-emitting devices [4], sensors [5] and imaging [6]. Fluorescent molecules responsive to various stimuli, such as photons [7], substances and environment (such as pH, water, and gas) [8], mechanical forces (mechanofluorochromism (MFC), piezochromism) [9–11] and aggregation-induced emission (AIE), [12] have been extensively studied [13–15]. Some of them are composed of functional receptor units and fluorescent emitter [16–18], where the receptor unit may have ion-, metal- or molecular-binding sites and modulate the fluorescence nature of the emitter depending on the stimulus. The exploration of new combinations of emitter and receptor units has thus been extensively studied.

Among various emitting units, difluoroboron derivatives such as DFB (difluoroboron β-diketonates) have been widely studied for their high fluorescence quantum yield, compatibility with various media, and sensitivity toward environmental conditions via the π-conjugation system with donor-acceptor feature and capability of hydrogen bonding at the BF_2 structure [19–23]. Specific MFC has also been reported for the DFB derivatives, in which mechanical smearing of powder samples displays significant fluorescence color and intensity changes [23–25]. Moreover, DFB with alkylamino and dialkylamino units have been reported to show pH sensitivity [26].

Despite these previous works, to our knowledge, DFB derivatives functionalized with a primary amino group have never been reported, while we may expect significant stimuli-responsivity of such compounds through hydrogen bonds and capability of protonation/de-protonation equilibrium and significant intramolecular charge transfer (ICT) [26]. In this paper, we report on the synthesis of difluoroboron 3-(4-aminophenyl)-1-(4-methoxyphenyl)propane-1,3-dione (**DFB-NH_2**) and its fluorescence properties in solution, polymer matrices, powder and single crystals. Despite its relatively simple structure, this molecule displays a unique multicolor fluorescence polymorphism, responsiveness toward mechanical stress, and an acidic and basic environment.

2. Results and Discussion

DFB-NH_2 was prepared via four-step synthesis (Figure 1). Firstly, Claisen condensation reaction of 4-methoxy acetophenone and dimethyl terephthalate was performed to obtain the β-diketonate **1**. Secondly, the carboxylic group of the β-diketonate was saponified with LiOH to obtain the carboxylic acid **2** following our previous procedure. [21] Thirdly, Curtius rearrangement with benzyl chloroformate (Cbz) was performed to obtain the β-diketonate with Cbz **3**, with a moderate yield.[27] Lastly, boronation on diketonate and deprotection of Cbz by boron trifluoride diethyl ether complex (BF_3OEt_2) was performed to obtain the target compound **DFB-NH_2** which was purified by reprecipitation and further by recrystallization for structural analysis. The detail of these steps is described in supporting information. It is worth

Journal Pre-proofs

mentioning that in our hands, a possible alternative route that would consist in the condensation of 4-methoxy acetophenone with Boc-protected methyl-4-aminobenzoate failed because the yield of the condensation product was very poor. To our knowledge, this represents the first example of the synthesis of DFB derivative functionalized with a primary amine. The newly synthesized molecule was characterized by ^{1}H, ^{13}C, ^{19}F NMR, and high-resolution mass spectrometry (Figure S1-S5).

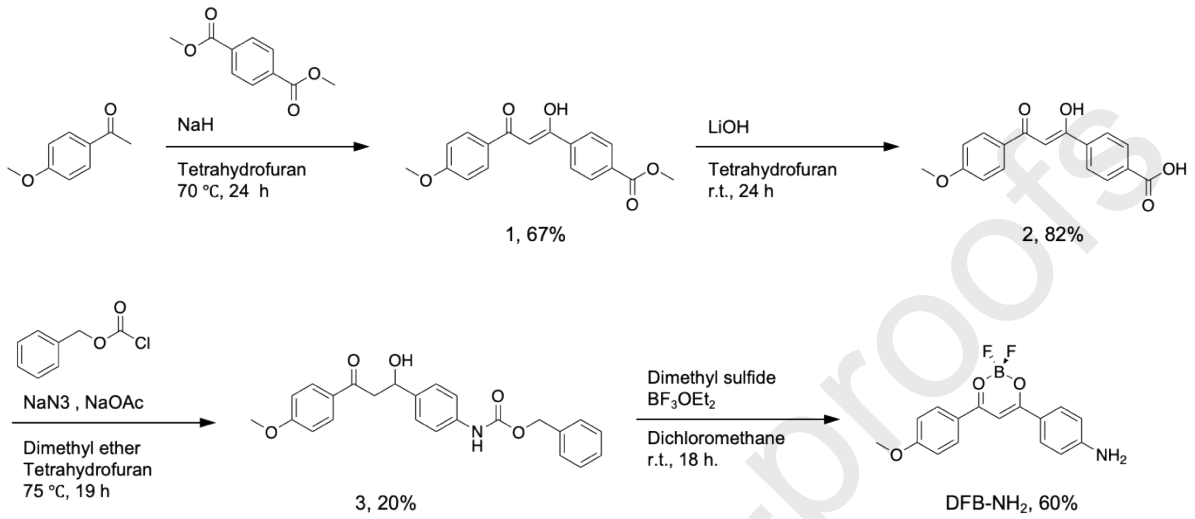

Figure 1. Synthetic route for ***DFB-NH$_2$.***

As shown in Figure 2, **DFB-NH$_2$** shows a characteristic absorption band at about 400 nm and emission at 450-500 nm in toluene and dichloromethane (DCM). The absorption, fluorescence emission and excitation spectra in some solvents are also presented in supporting material (Tables 1 and Figure S6(a) and (d)). In the following discussion, we mostly focused on the emission behaviour in DCM and toluene. The molar absorption coefficient (ε) was measured in DCM as 6.42×10^{4} L mol^{-1} cm^{-1}, which is similar to other DFB derivatives (see Table 1). [25] The fluorescence quantum yield ($\boldsymbol{\Phi}_{\mathbf{F}}$) was measured as $\boldsymbol{\Phi}_{\mathbf{F}}$=0.95 and 0.91 in toluene and DCM, respectively. $\boldsymbol{\Phi}_{\mathbf{F}}$ values of **DFB-NH$_2$** above 0.9 seem to be relatively high among DFB derivatives. [25] The rigid and planar structure due to the coordination of the two carbonyl groups and fluorine atom by boron atom should contribute to these high $\boldsymbol{\Phi}_{\mathbf{F}}$. We will present DFT (Density Functional Theory) calculation results in the following section. We further investigated emission decay profiles with single-component kinetics in toluene with τ=1.79 ns at 450 nm and also in DCM with τ=2.06 ns at 510nm (see Table 1 and Figure S6). Two-component decay was observed in DCM at 450nm, τ_1=1.96 nsec(85%) and τ_2=1.00 nsec(15%), from which <τ>=1.81 nsec was derived as an average value. Because the contribution of the minor component was only 15%, the average time constant <τ> was utilized for calculating the kr values (kr = 5.0×10^{-8} s^{-1}), which is similar to that of toluene (5.3×10^{-8} s^{-1}).

The single and two-component emission decay feature in DCM depending on the emission wavelength is attributable to the contributions of locally-excited (LE) higher energy state and low-lying ICT state with co-planar structure for the large $\boldsymbol{\Phi}_{\mathbf{F}}$ [26]. Two component emission was also observed in THF with shorter and longer emission wavelength (435 nm, 490 nm) and two emission decay components (τ_1 = 0.38 ns (98%), τ_2 = 1.42 (2%) ns at 450 nm, τ_1 = 0.44 ns (53%), τ_2 = 1.63 (47%) ns at 530 nm, Figure S6(c) and (d)).

Journal Pre-proofs

*Table 1. Photophysical properties of **DFB-NH$_2$** in solution in toluene, dichloromethane (DCM), before and after addition of trifluoroacetic acid (TFA).*

Solvent	Maximum wavelength [nm]			ε [L mol^{-1} cm^{-1}]	Φ_F (λ_{ex})	τ [ns] (λ_{em}= 450 nm)	k_r [s^{-1}]	k_{nr} [s^{-1}]
	Emission (λ_{ex}=410 nm)	Absorption	Excitation (λ_{em}=480 nm)					
Toluene	458	428	425	-	0.95 (415)	1.79	5.3×10^{-8}	2.8×10^{-11}
Toluene + TFA	460	400	395	-	-	1.34	-	-
DCM	476	430	430	6.42×10^4	0.91 (420)	1.81 *1)	5.0×10^{-8} *21)	5.0×10^{-11} *2)
DCM + TFA	460	395	397	-	-	1.26	-	-

1) an average lifetime value for two lifetimes. 2) based on the average lifetime

Since **DFB-NH$_2$** possesses an amino group, it is sensitive to acidic conditions. In order to characterize the acid detection properties, an excess amount of trifluoroacetic acid (TFA) was added to DCM and toluene solution (Figure 2). As summarized in Table 1, adding TFA leads to a blue shift in the absorption and excitation spectra for both toluene and DCM. However, the emission properties showed no significant change upon the addition of TFA in toluene (Figure 2 (a), (c), and (e)). In the DCM solution, while, TFA triggered blue fluorescence (Figure 2 (b) and (d)), accompanying hypsochromic shift of the emission peak from 476 nm to 460nm (Figure 2 (f)). The lifetime also changed from 1.81 ns to 1.26 ns (Figure 2 (h)). The significant solvent dependence in emission properties of **DFB-NH$_2$** is attributed to the typical ICT nature in DCM solution, which should be diminished in the protonated form, **DFB-NH$_3^+$**. On the

contrary, in toluene, **DFB-NH$_2$** predominantly exhibits emission from LE state prior to the addition of TFA, which is similar state to **DFB-NH$_3^+$**.

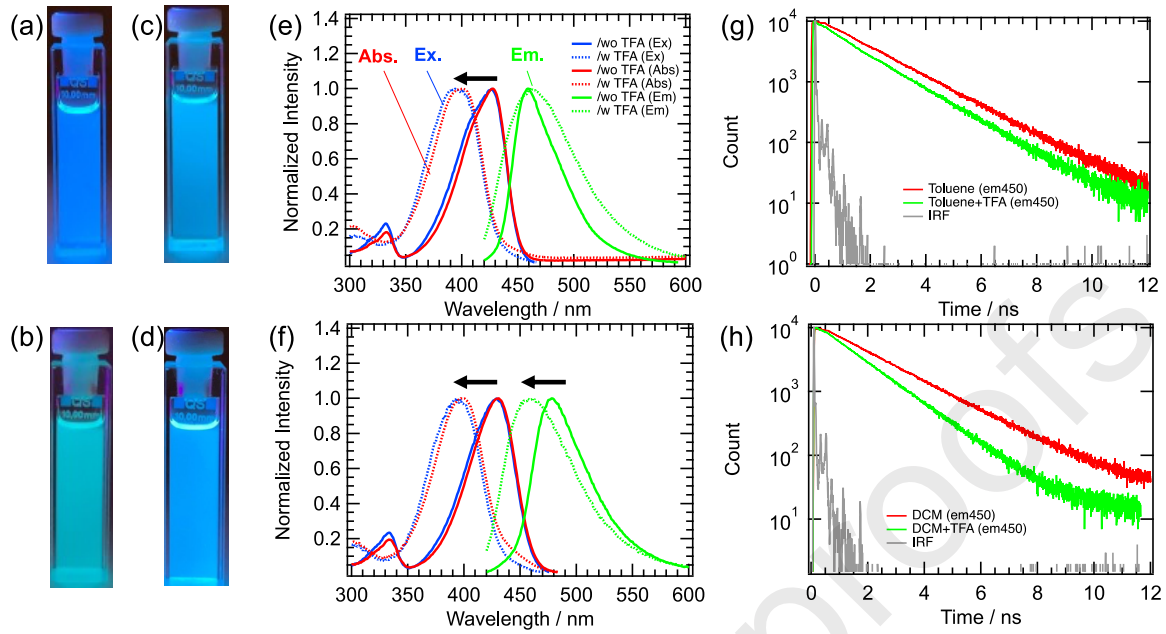

Figure 2. Fluorescence properties of ***DFB-NH$_2$*** *in solution, on top: in toluene, bottom: in DCM, and* effects of TFA. *Fluorescence image of* ***DFB-NH$_2$*** *(a) in toluene, (b) in DCM, (c) in toluene+TFA, and (d) in DCM + TFA. Fluorescence emission (λ_{ex}=410 nm, green), absorption (red), excitation (λ_{em} =490 nm, blue) spectra (e) in toluene and (f) in DCM, w(dotted-line)/wo(solid-line) TFA. Fluorescence decays (g) in toluene and (h) in DCM, before and after adding TFA (λ_{ex}=390 nm, λ_{em} =450 nm).*

According to previous studies, a polymer matrix can segregate solutes and provide information about the photophysical properties of compounds isolated in a photochemically inert matrix. [28] In other words, a polymer medium can create a solute-dispersed environment similar to the solution. To investigate acid and base responsive properties, polymer dispersed sample was also investigated. Polymethyl methacrylate (PMMA) was selected as a polymer medium. By following the method shown in Section 5, 0.07 wt% dye-doped PMMA film was prepared. The film initially had a cyan-blue color, and a fluorescence peak at 470 nm was obtained (Figure 3 (a), (d)). Next, the acid-base sensing ability was investigated. After exposure to TFA and NH_3 vapour, the fluorescence color and spectral change were monitored. Firstly, the film was placed in a small container with saturated TFA vapours for 5 minutes. When the film was exposed to TFA, the fluorescence color changed from cyan-blue, and the fluorescence peak changed from 470nm to 420nm (2530 cm^{-1} shift) (Figure 3 (b), (d)). After that, the film was exposed to NH_3 vapour for 5 minutes. The fluorescence color went back to the original cyan-blue, and its fluorescence emission maximum changed to 480 nm (Figure 3 (c), (d)). From this result, the solution color of **DFB-NH$_2$** can be fixed in the polymer film. The film can also exhibit acid and base sensing properties, which benefits the application towards flexible acid and base sensors.

Journal Pre-proofs

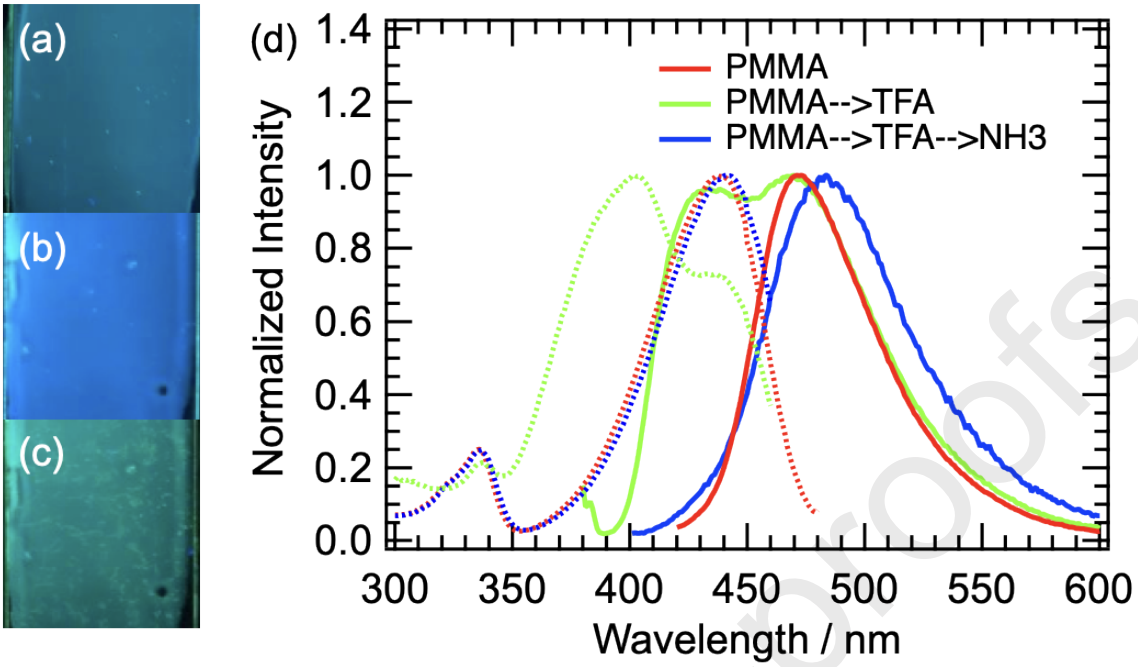

Figure 3. Photophysical properties of ***DFB-NH$_2$*** *in PMMA (*0.07 wt%*). Fluorescence image of (a)* ***DFB-NH$_2$*** *doped PMMA film, (b) After exposing to TFA vapours, (c) After exposing to NH_3 vapours (b), (d) Fluorescence and excitation spectra (λ_{ex}=400 nm, λ_{em} =495 nm).*

A single crystal of **DFB-NH$_2$** was obtained by the slow evaporation method with DCM and hexane. Red needle-shaped crystals were obtained (Figure S12). To understand the molecular packing of **DFB-NH$_2$**, an X-ray diffraction analysis was performed. Figure 4 shows the single-crystal structure of **DFB-NH$_2$**. An anti-parallel alignment of neighbouring molecules forming a dimer structure was observed. As summarized in Table S1, the crystal belongs to a crystal system of *P 21/c* space group, and the unit cell contains four nearly coplanar molecules. As shown in Figure 4 (a) and (b), the aligned anti-parallel dimers make columnar stacking. The distance of the two anti-parallel molecules in the dimer was taken as the distance between the centroids of aromatic rings (Figure 4(c)). The value was calculated to be 3.73 Å, corresponding to the π-stacking interaction. Neighbouring dimers are tethered by specific NH/F interactions (see Figure 4 (e), F…HC; 2.66 Å. F…HN; 2.68 Å, Figure 4 (f), F…HC; 2.54 Å. F…HN; 2.41 Å). The dimer-dimer distance was calculated as 4.06 Å (see Figure 4 (d)) from the centroid distance of stacking phenyl rings. The slip-stacking dimers promote a hydrogen bonding network. These results suggest that the crystal of **DFB-NH$_2$** is constructed by several weak interactions between dimers, which might be disturbed by external stimuli [29].

Journal Pre-proofs

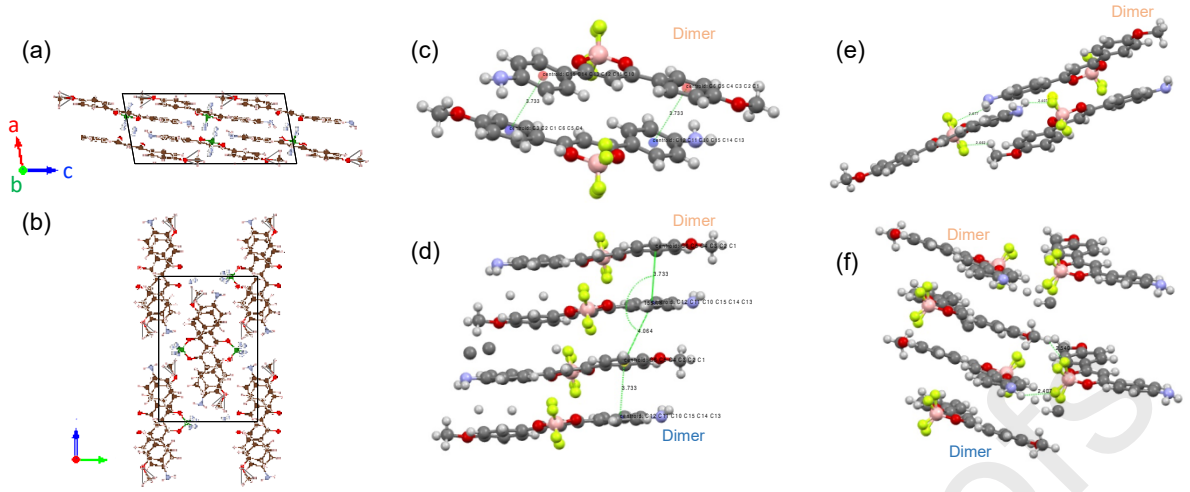

Figure 4. Single crystal structure of ***DFB-NH$_2$****. (a) packing view along b axis, (b) packing view along an axis, (c) distance between two molecules which construct a dimer, (d) distance between two dimers, (e) distance between a dimer and a neighbouring molecule, (f) distance of a molecule which mediates two dimers.*

We subsequently investigated the luminescence properties of **DFB-NH$_2$** in solid state (crystalline and powder) to compare them with its solution-phase behaviour. Figure 5(a) shows a photographic image of single crystals under UV light irradiation (365 nm) with dark-red luminescence. The emissivity of **DFB-NH$_2$** molecules in the solution phase is efficiently suppressed in the crystal structure, which is composed of π-stacking anti-parallel dimer structure. The significant effect of the H-type dimerized structure is also notable in the bathochromic shift of the emission band to 624 nm, which is much longer than the solution and polymer dispersed films and is primarily attributable to the excitonic interaction in the dimer. Excited state interaction between the dimers may also contribute to this emission wavelength shift. As shown in Figure 5(c), the drop cast of acetone solution onto a filter paper produced powder-like samples with fluorescence emission at about 580 nm. In this deformed polycrystalline state, we could observe much higher emissivity. Although their structure-property relationship is not fully characterized here, they suggest the polymorphic nature of **DFB-NH$_2$** in the solid state. In the drop-casted sample, a part of **DFB-NH$_2$** should form a bright emissive phase. Thus, even if some parts are still in the *dark-red* crystal particles, they may not be detected under UV light. The single crystal and powder samples were then smeared, and their fluorescence properties were studied. The emission of the single crystal at 624 nm shifted to 600 nm (Figure 5(a), (b), (e)) after smearing. Moreover, the powder X-ray diffraction pattern (Figure S11) revealed that the pattern became much broader after grinding, suggesting that this transition corresponds to a shift from crystalline to amorphous. The drop-casted powder with orange emission (Figure 5 (c)) at λ_{em}=575 nm also demonstrated MFC nature after smearing, with yellow emission at λ_{em}=542 nm (Figure 5 (d), (e)). Interestingly, **DFB-NH$_2$** indicated a blue shift in the emission wavelength and enhanced emission properties after smearing in both sample systems. In typical MFC behaviour of DFBs, the fluorescence displays red shifts after smearing [23,24,30]. This phenomenon should originate from changes in the packing structure

of the fluorophores favouring the appearance of strong π-π interactions and excimer structures, with disruption of the hydrogen bonds network between F and αH atoms. Due to these structural changes, emissive materials newly form in the mechanically perturbed areas, resulting in red-shifted emission in the amorphous state[24]. The excited state energy migration in the partially deformed amorphous solid state may also contribute to the red-shifted emission. Meanwhile, there are limited reports of the opposite type of MFC, i.e. blue-shifted MFC [29,31,32]. Chen *et al.* reported, for example, that carbazole-containing difluoroboron β-diketonate showed blue-shifted MFC. They explained those emission changes saying that the grinding process was disrupting the crystalline order and leading to reduced excitonic delocalization [29]. Another study by Yamaguchi *et al.* focused on a tetrathiazolylthiophene derivative and its behaviour when subjected to anisotropic forces. When such forces were applied, the emission properties of the compound undergo a significant blue shift attributed to the disruption of the H-bond network and the disintegration of dimer packing, leading to a less ordered arrangement.[33] Based on these studies, the hypsochromic-shifted MFC in **DFB-NH$_2$** crystal could be linked to the deformation of the initial packing structure. As a related matter, we have previously observed a blue shift in luminescence at the nanoscale, which was ascribed to a crystal-to-crystal phase transition triggered by forces applied through an AFM tip. This contrasts with the red-shifted MFC in macroscale in the same system. However, we assume that a different mechanism underlies in the case of **DFB-NH$_2$**, as the present transition corresponds to a crystal-to-amorphous state. [34] We here notice the importance of the anti-parallel dimer arrangement in the crystal lattice, which efficiently promotes the red-shifted emission in the crystalline state, with notably decreased luminescence intensity compared to the solution phase. This may be attributed to the partial symmetry forbidden effect of the H-type dimer. The structural deformation after mechanical stimulation and blue-shifted emissions can be explained by the disruption of those anti-parallel H-type dimer structure which goes along with the emission intensity increase as observed. Although ideal H-type dimers have been theoretically predicted to be non-emissive, practical crystals may show dark red emission.[35] Spano and coworkers have recently reported a significant contribution of quadrupolar interaction in H-type dimers of DAD-type molecules, resulting in red-shifted emission of H-type dimer aggregates.[36]

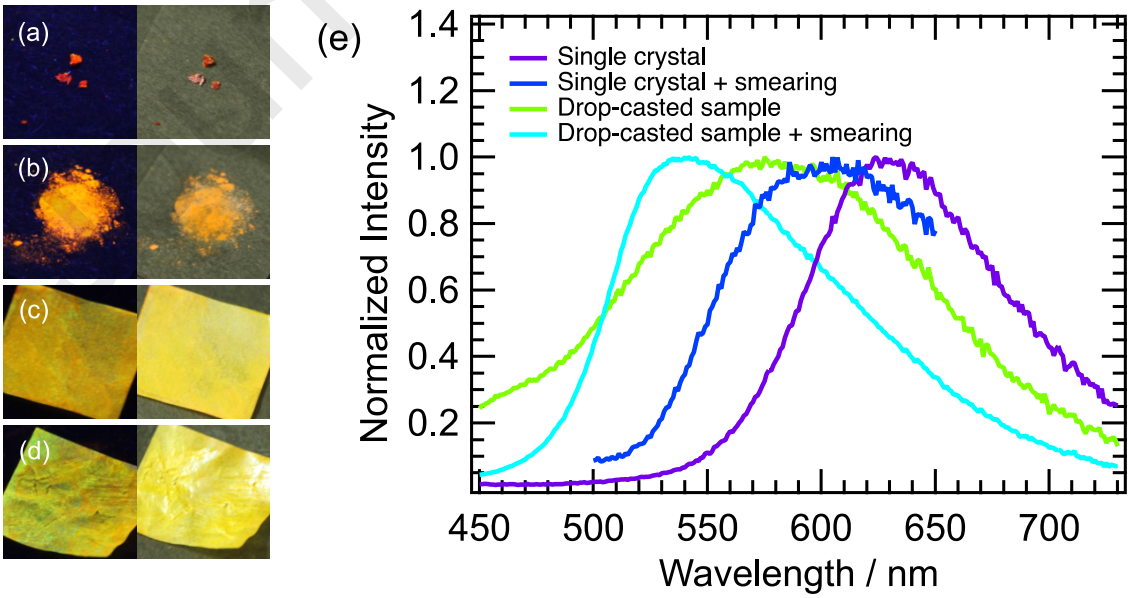

Journal Pre-proofs

Figure 5. Photophysical properties of ***DFB-NH$_2$*** *in solid-state. Images under UV (365nm, right) and ambient light (left) of (a) single crystal, (b) after smearing of (a), (c) drop-casted sample on paper from acetone solution, (d) after smearing of (c). (e) Fluorescence spectra (λ_{ex}=400 nm), purple, blue, green, light blue curves correspond to (a), (b), (c), and (d) respectively. For the spectrum of "Single crystal + smearing", the representing wavelength region is limited in order to avoid the light scattering effect.*

An acid- and base-detection was further studied with pure **DFB-NH$_2$** powder using similar conditions to the polymer dispersed sample (Figure 6). As a related topic, Chujo et al. have reported clear acid-base responsive boron diiminate-containing polymer films [37,38]. We here demonstrate similar experiments with polycrystalline molecular powders [39]. Before acid exposure, the bulk crystal showed red emission at 624 nm (Figure 6 (a), (d)). The red crystal was placed into a small glass vessel with saturated TFA vapour for 5 min. The crystal color changed immediately while melting and changing shape. The fluorescence color changed to yellow, and the fluorescence spectra maximum shifted to 573 nm (Figure 6 (b), (d)). After that, the crystal was exposed to NH_3 vapour for 5 min. The fluorescence color returned to red, and the fluorescence spectral peak was back to 624 nm (Figure 6 (c), (d)). These results clearly show that the acid- and base-sensing properties are reversible even in the bulk solid state.

The possible molecular-level scheme is illustrated in Figure 6 (e). Before TFA exposure, the primary amine, the boron chelate ring, and the methoxy might act as a strong donor, an acceptor, and a weak donor, respectively, leading to the observed red emission. On the contrary, after protonation, the primary amine, the boron chelate ring, and the methoxy might act as an acceptor, an acceptor, and a weak donor, respectively. The strong donor-acceptor interactions between the primary amine and the boron-chelating ring are expected to be suppressed by the protonation of the amino group, promoting a much blue-shifted emission in acidic conditions. We also observed partial shape change of powder with small transparent portion after exposing the sample to TFA vapours. Two terms may simultaneously contribute to this partial melting phenomenon, to which water in the air may contribute in some extent. TFA may contribute to break the hydrogen bonds and other short-contact interactions between neighbouring molecules, causing the crystal lattice to weaken. The TFA may also form TFA-water liquid phase with **DFB-NH$_3^+$/DFB-NH$_2$** molecules, leading to deliquescence.

Journal Pre-proofs

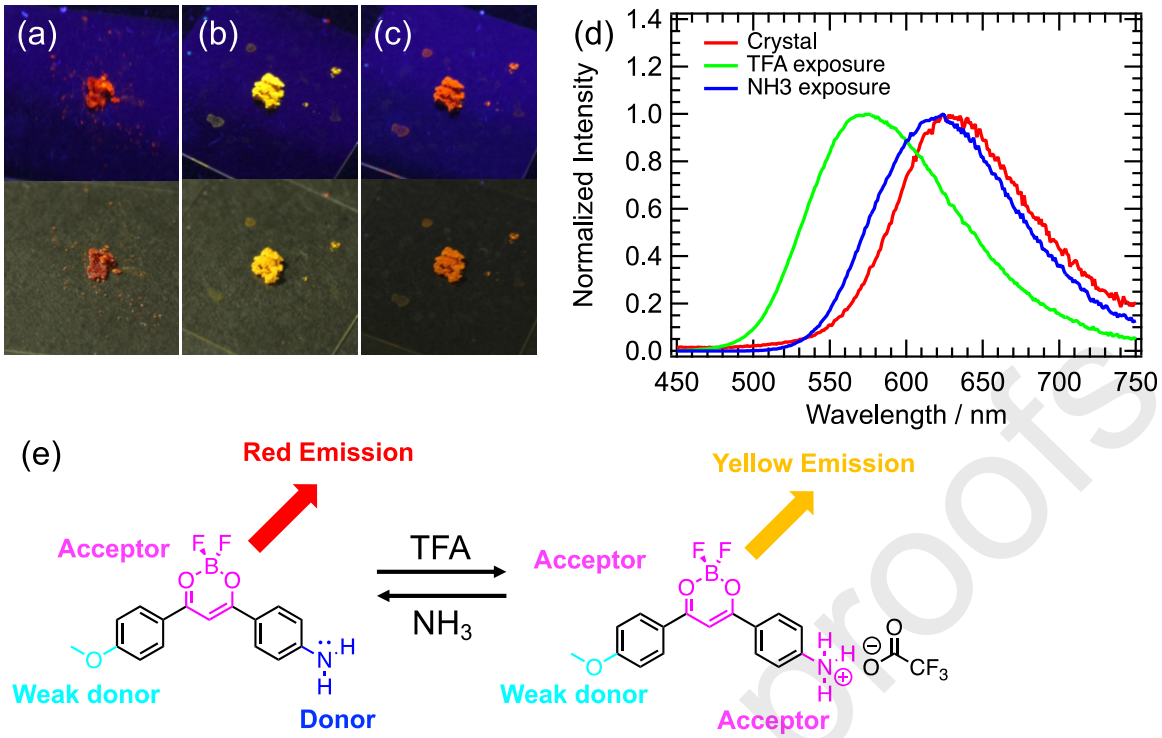

*Figure 6. Acid and base sensitive properties of **DFB-NH$_2$** in the solid state. Images under UV (365nm, top) and ambient light (bottom) of (a) the initial single crystal, (b) the solid after TFA exposure, (c) the solid after NH_3 exposure. (d) Fluorescence spectra (λ_{ex}=410 nm): red = crystal, green = after TFA exposure, blue = after NH_3 exposure. (e) Scheme of the pH-responsive behaviour of **DFB-NH$_2$** in solid.*

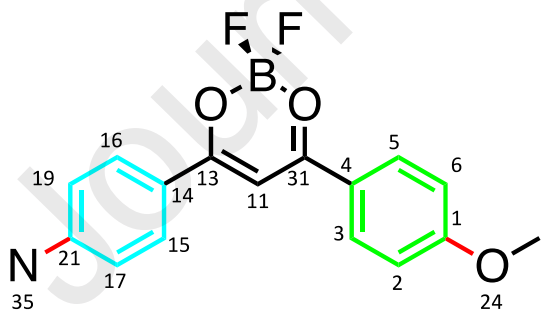

*Figure 7. Molecular structure of **DFB-NH$_2$** with numbering of each atom.#35-N may connect to two or three H atoms.*

Journal Pre-proofs

Journal Pre-proofs

Journal Pre-proofs

Table 2. Correlation of bond distances between the crystal structure and the calculated data (neutral form in DCM, acidic form in DCM+H^+). The atomic number corresponds to Figure 7. The color in the table corresponds to the bond color in the Figure 7.

Atomic number	Bond distance [Å]		
	DCM	**DCM+H^+**	**Crystal**
21,35	1.3631	1.4757	1.367
17,21	1.4099	1.3843	1.403
19,21	1.4094	1.3862	1.408
16,19	1.3777	1.3869	1.365
15,17	1.3780	1.3887	1.369
14,16	1.4071	1.3987	1.404
14,15	1.4069	1.3964	1.407
1,2	1.4023	1.4039	1.395
2,3	1.3790	1.3769	1.369
3,4	1.4059	1.4082	1.411
4,5	1.3985	1.4016	1.393
5,6	1.3879	1.3849	1.387
1,6	1.3975	1.3998	1.397
1,24	1.3498	1.3444	1.356

Journal Pre-proofs

Journal Pre-proofs

To understand the acid-base responsive nature of **DFB-NH$_2$**, we performed DFT calculations using the CAM-B3LYP hybrid functional and the 6-31+G(d,p) basis set. We studied the optimized geometry and the correlation between the calculated structure and the X-ray diffraction data. First, as shown in Figure S7, the optimal structure of **DFB-NH$_2$** is almost a coplanar structure. Moreover, as shown in Figure 7 and Table 2, a quinoid-like structure was observed on the two benzene rings, especially on the amide side. Concretely, the bond distance of C16-C19 (1.38 Å) and C15-C17(1.38 Å) is notably shorter than the bond distance of C19-C21 (1.41 Å), C17-C21 (1.41 Å), C14-C16 (1.41 Å), and C14-C15 (1.41 Å). We found the same trend in X-ray diffraction data. Moreover, according to the DFT calculation, the molecule showed a stronger quinoid effect in DCM than in toluene (see Table S2). The DFT calculation also provided sp^2-like co-planar structure around the N atom in **DFB-NH$_2$**, as we obtained the sum of three internal bond angles (<CNH, <HNH, <HNC) around the primary amine N-atom as 355.1^o. These quinoid-like structures, associated with a significant CT state, support the C=NH_2^+ character of the amino group (Figure S10).

Next, we investigated the differences between the optimized geometries of **DFB-NH$_2$** and **DFB-NH_3^+.** It can be noticed that the bond distance of C21-N35 is shorter in the neutral form than in the protonated form, which is also consistent with the contribution of the C=N quinoid structure in **DFB-NH$_2$** but not in **DFB-NH_3^+**. We also investigated the angle between the chelate and benzene rings (Figure S7, Table S3). The benzene ring (**A**) on the NH_2 side and (**C**) on the OMe side were studied through their twisting angles with respect to the central O-B-O chelate ring (**B**). In DCM, the angles θ_{AB}=1.98 º and θ_{BC}=5.60 º for **DFB-NH$_2$** change to θ_{AB}=11.9 ºand θ_{BC}=3.92 º for **DFB-NH_3^+**. This notable change in θ_{AB} suggests a suppression of the quinoid contribution around the A-ring in **DFB-NH_3^+**. Unfortunately, this discussion is not fully consistent with the observed twisting angles in the crystal structure, which could be explained by the intermolecular interactions in the crystal.

Moreover, the calculated UV-vis spectra and fluorescence vertical transitions, energy of HOMO and LUMO are reported in Table S4 and Figure S8. HOMO and LUMO electric transition dipole moments are also characterized by time-dependent density function theory (TD-DFT) calculation, and spectra calculations successfully reproduce the blue-shifted absorption after protonation of **DFB-NH$_2$**.

3. Conclusion

In conclusion, a novel DFB compound functionalized with a primary amine, **DFB-NH$_2$,** was successfully obtained. **DFB-NH$_2$** has a significantly high fluorescence quantum yield in toluene and DCM. Also, it shows acidochromic properties in solution, dispersed in PMMA film and in powder form. The condensed state also shows unusual blue-shifted mechanofluorochromism, probably due to the D-A-D' structure and its compact and H-type crystal packing form. Based on these results, **DFB-NH$_2$** exhibits a wide range of color changes from blue to red and efficient responsivity to multiple stimuli.

Journal Pre-proofs

4. Acknowledgements

This project received funding from the European Research Council (ERC) under the European Union Horizon 2020 research and innovation program (grant agreement No. 715757 MECHANOFLUO to C.A.). We would like to acknowledge Nara Institute of Science and Technology, Division of Materials Science, Photonic and Reactive Molecular Laboratory and ENS-Paris Saclay Laboratoire de Photophysique et Photochimie Supramoléculaires et Macromoléculaires (PPSM) for the financial support. This study was supported by JSPS KAKENHI Grant Number 23H04876, belong to *Mesohierarchy* program. This work was performed using HPC resources from the "Mésocentre" computing center of CentraleSupélec and École Normale Supérieure Paris-Saclay supported by CNRS and Région Île-de-France (http://mesocentre.centralesupelec.fr/). We also thank Ms. Y. Nishikawa and Mr. F. Asanoma, at Center for Material Research Platform, CMP, for their technical research support on MS- and NMR-measurements. M.L. thank the NAIST Foundation for their financial support. S.K. acknowledges Japan Chemical Industry Association for their scholarship support with the Chemistry Personnel Cultivation Program. This study was also supported by the LIA Nanosynergetics program, CNRS.

5. Materials and methods

Analytical reagents were purchased from Tokyo Chemical Industry Co., Ltd (TCI), Sigma Aldrich, and Wako Pure Chemical Industries, Ltd. These chemicals were used without further purification. The reactions were monitored using Merck TLC silica gel 60 F254 and visualized using UV lamp with wavelength 254 nm and 365 nm. ^{1}H, ^{13}C, and ^{19}F NMR analyses were recorded using 400MHz, 500MHz NMR JEOL JNM-ECX-500 and 600MHz NMR JEOL JNM-ECA600. The molecular mass was analyzed by using high Bruker Autoflex II MALDI-TOF and JEOL MALDI Spiral-TOF high resolution mass spectrometer.

All absorption and emission measurements were conducted using spectroscopy grade solvent purchased from Carlo Erba without any purification, except for THF, which was not at spectroscopic grade but dried before use. The absorption spectra were recorded by using double-beam spectrophotometers Cary 100 or Cary 4000 from Agilent Technologies. The emission spectra were measured using Horiba Jobin-Yvon spectrofluorometers Fluoromax FM3 and Fluorolog FL3-221. The fluorescence quantum yield of **DFB-NH$_2$** was determined by relative quantum yield measurement with Coumarin 153 as a standard sample (literature $\boldsymbol{\Phi}_F(0) = 0.54$). For solid state, fluorescence spectra were measured by FluoroLog3 equipped with optical fibers. The excitation wavelength was set at 400nm. The compound was deposited either on paper or glass.

Fluorescence decay curves were obtained by the time-correlated single-photon counting (TCSPC) method. The setup is composed of a titanium sapphire Ti:Sa oscillator (Spectra Physics, Maï Taï HP) emitting pulses of 100 fs duration at 780 nm, 80 MHz frequency. The laser pulses then pass through a pulse picker to reduce the repetition rate at 4 MHz. The signal is doubled at 390nm by focalising the laser in a non-linear SHG crystal (GWU Lasertechnik, UHG-23-PSK). Then the beam passes through the sample solution after adjusting the excitation power with an intensity attenuator filter wheel. Fluorescence photons are detected at 90° through a monochromator (CVI Laser Corporation, Digikröm CM110) and a polarizer at magic angle by means of a micro channel plate photomultiplier (Hamamatsu, MCP-PMT R3809U-50), connected to a TCSPC module (Becker & Hickl, SPC-130-EMN). The instrumental

Journal Pre-proofs

response function is recorded before each decay measurement with a fwhm (full width at halfmaximum) of ~25 ps. Time-correlated fluorescence decay data are finally processed and analysed with the help of a software which implements the non-linear square method (Globals, Laboratory for Fluorescence Dynamics at the University of California, Irvine).

Solution preparation: 1×10^{-6} M toluene or DCM solution was prepared. For the acid sensitivity test, 0.1 mL (1.3 mmol) of TFA was added to 3 mL of toluene or DCM solution.

Polymer sample preparation: 5g of PMMA was dissolved in 45 g of toluene, preparing 10 w% PMMA/toluene solution. 70 mg **DFB-NH$_2$** was dissolved in 1 g of 10 w% toluene/PMMA solution. The solution was dropped on a glass slide, preparing 0.07 w% dye-doped PMMA film. The drop was deposited using an automatic film applicator from TQC and dried for one day.

Acidochromism test: the polymer film or the crystal deposited on a glass slide was placed in a small container with TFA. The container was covered to make a saturated atmosphere, and the sample was exposed to TFA for 5 min and dried for 5 min. After vapouring TFA, the fluorescence spectrum was measured. Then it was exposed to NH_3 fumes for 5 min and dried for 5 min. The fluorescence spectrum was then measured.

DFB-NH$_2$ crystals were obtained by a slow evaporation process starting from a saturated DCM solution. A suitable single crystal was isolated and mounted in a sample holder. X-ray diffractions were recorded using Rigaku Varimax Rapid RA Micro7 equipped with an imaging plate detector monochromated Mo Kα radiation at 103.15 K. The crystal structure and calculations were done using the system software Rigaku Crystal structure 3.8.1. Mercury 2022 3.0 software and VESTA were applied to analyse and visualise crystal structure. The deposition number 2285179 (for **DFB-NH$_2$**) contains the supplementary crystallographic data for this paper.

The geometry of compounds **DFB-NH$_2$** and **DFB-NH$_3^+$** have been fully optimized by the DFT method by using CAM-B3LYP functional with 6-31+G(d,p) basis set as implemented in the Gaussian 16 software package. Frequency calculations were performed to confirm that the geometries obtained correspond to energy minima. Implicit solvent model IEFPCM was used. Franck−Condon energy transitions were calculated by TD-DFT with the same functional and basis set.

References

[1] J.R. Lakowicz, Principles of Fluorescence Spectroscopy, Springer US, 2006.

[2] B. Valeur, Molecular Fluorescence: Principles and Applications, Wiley & Sons, Incorporated, John, 2001.

[3] Z. Chi, X. Zhang, B. Xu, X. Zhou, C. Ma, Y. Zhang, S. Liu, J. Xu, Recent advances in organic mechanofluorochromic materials, Chem. Soc. Rev. 41 (2012) 3878–3896.

[4] S.-C. Lo, P.L. Burn, Development of dendrimers: macromolecules for use in organic light-emitting diodes and solar cells, Chem. Rev. 107 (2007) 1097–1116.

[5] Z. Hu, B.J. Deibert, J. Li, Luminescent metal–organic frameworks for chemical sensing and explosive detection, Chem. Soc. Rev. 43 (2014) 5815–5840.

[6] R. Jenkins, M.K. Burdette, S.H. Foulger, Mini-review: fluorescence imaging in cancer cells using dye-doped nanoparticles, RSC Adv. 6 (2016) 65459–65474.

[7] J. Zhang, Q. Zou, H. Tian, Photochromic materials: more than meets the eye, Adv. Mater. 25 (2013) 378–399.

[8] R. Kumari, M.D. Milton, Design and synthesis of multi-stimuli responsive π-extended phenothiazine aldehydes: Solvatochromism, acidochromism, moisture detection and fluorochromic sensing of amine vapors, Dyes Pigm. 205 (2022) 110474.

[9] C. Wang, Z. Li, Molecular conformation and packing: their critical roles in the emission performance of mechanochromic fluorescence materials, Mater. Chem. Front. 1 (2017) 2174–2194.

[10] Y. Sagara, S. Yamane, M. Mitani, C. Weder, T. Kato, Mechanoresponsive Luminescent Molecular Assemblies: An Emerging Class of Materials, Adv. Mater. 28 (2016) 1073–1095.

[11] Y. Sagara, T. Kato, Mechanically induced luminescence changes in molecular assemblies, Nat. Chem. 1 (2009) 605–610.

[12] Y. Hong, J.W.Y. Lam, B.Z. Tang, Aggregation-induced emission, Chem. Soc. Rev. 40 (2011) 5361–5388.

[13] A. Abdollahi, H. Roghani-Mamaqani, B. Razavi, Stimuli-chromism of photoswitches in smart polymers: Recent advances and applications as chemosensors, Prog. Polym. Sci. 98 (2019) 101149.

[14] D. Yan, D.G. Evans, Molecular crystalline materials with tunable luminescent properties: from polymorphs to multi-component solids, Mater. Horiz. 1 (2013) 46–57.

[15] Y. Ke, J. Chen, G. Lin, S. Wang, Y. Zhou, J. Yin, P.S. Lee, Y. Long, Smart windows: Electro-, Thermo-, mechano-, photochromics, and beyond, Adv. Energy Mater. 9 (2019) 1902066.

[16] W. Li, Y.-M. Zhang, T. Zhang, W. Zhang, M. Li, S.X.-A. Zhang, Tunable RGB luminescence of a single molecule with high quantum yields through a rational design, J. Mater. Chem. 4 (2016) 1527–1532.

[17] T. Inouchi, T. Nakashima, T. Kawai, Acid-base-responsive intense charge-transfer emission in donor-acceptor-conjugated fluorophores, Chem. Asian J. 9 (2014) 2542–2547.

[18] A. Zavaleta, A.O. Lykhin, J.H.S.K. Monteiro, S. Uchida, T.W. Bell, A. de Bettencourt-Dias, S.A. Varganov, J. Gallucci, Full Visible Spectrum and White Light Emission with a Single, Input-Tunable Organic Fluorophore, J. Am. Chem. Soc. 142 (2020) 20306−20312.

[19] F. Ito, R. Naganawa, Y. Fujimoto, M. Takimoto, Y. Mochiduki, S. Katsumi, Real-Time

Journal Pre-proofs

Fluorescence Visualization of Nanoparticle Aggregation and the Polymorph-Transition Process of a Mechanofluorochromic Difluoroboron-β-Diketone Derivative, ChemPhysChem. 22 (2021) 1.

[20] S. Katsumi, M. Saigusa, F. Ito, Molecular Aggregation Dynamics via a Liquid-like Cluster Intermediate during Heterogeneous Evaporation as Revealed by Hyperspectral Camera Fluorescence Imaging, J. Phys. Chem. B. 126 (2022) 976–984.

[21] J.A. Panis, M. Louis, A. Brosseau, S. Katao, F. de Los Reyes, T. Nakashima, R. Métivier, C. Allain, T. Kawai, Circularly Polarized Luminescence and Circular Dichroism of Bichromophoric Difluoroboron-β-diketonates: Inversion and Enhanced Chirality Based on Spatial Arrangements and Self-Assembly, Chemistry. 28 (2022) e202201012.

[22] B. Poggi, E. Lopez, R. Métivier, L. Bodelot, C. Allain, Mechanofluorochromic Difluoroboron β-diketonates based Polymer Composites: Towards Multi-Stimuli Responsive Mechanical Stress Probes, Macromol. Rapid Commun. (2022) 2200134.

[23] G. Zhang, J. Lu, M. Sabat, C.L. Fraser, Polymorphism and reversible mechanochromic luminescence for solid-state difluoroboron avobenzone, J. Am. Chem. Soc. 132 (2010) 2160–2162.

[24] L. Wilbraham, M. Louis, D. Alberga, A. Brosseau, R. Guillot, F. Ito, F. Labat, R. Métivier, C. Allain, I. Ciofini, Revealing the Origins of Mechanically Induced Fluorescence Changes in Organic Molecular Crystals-support, Adv. Mater. 30 (2018) e1800817.

[25] P.-Z. Chen, L.-Y. Niu, Y.-Z. Chen, Q.-Z. Yang, Difluoroboron β-diketonate dyes: Spectroscopic properties and applications, Coord. Chem. Rev. 350 (2017) 196–216.

[26] J. Hu, Z. He, Z. Wang, X. Li, J. You, G. Gao, A simple approach to aggregation-induced emission in difluoroboron dibenzoylmethane derivatives, Tetrahedron Lett. 54 (2013) 4167–4170.

[27] H. Lebel, O. Leogane, Curtius rearrangement of aromatic carboxylic acids to access protected anilines and aromatic ureas, Org. Lett. 8 (2006) 5717–5720.

[28] F. Ito, H. Sato, Y. Ugachi, N. Oka, S. Ito, H. Miyasaka, Properties and evolution of emission in molecular aggregates of a perylene ammonium derivative in polymer matrices, Photochem. Photobiol. Sci. 14 (2015) 1896–1902.

[29] P.-Z. Chen, J.-X. Wang, L.-Y. Niu, Y.-Z. Chen, Q.-Z. Yang, Carbazole-containing difluoroboron β-diketonate dyes: two-photon excited fluorescence in solution and grinding-induced blue-shifted emission in the solid state, J. Mater. Chem. C. 5 (2017) 12538–12546.

[30] M. Louis, A. Brosseau, R. Guillot, F. Ito, C. Allain, R. Métivier, Polymorphism, Mechanofluorochromism, and Photophysical Characterization of a Carbonyl Substituted Difluoroboron-β-Diketone Derivative, J. Phys. Chem. C. 121 (2017) 15897–15907.

[31] B. Wang, Z. Wu, B. Fang, M. Yin, Blue-shifted mechanochromism of a dimethoxynaphthalene-based crystal with aggregation-induced emission, Dyes Pigm.

182 (2020) 108618.

[32] Y. Hirai, L. Laize-Générat, A. Wrona-Piotrowicz, J. Zakrzewski, A. Makal, A. Brosseau, L. Michely, D.-L. Versace, C. Allain, R. Métivier, Multi-Directional Mechanofluorochromism of Acetyl Pyrenes and Pyrenyl Ynones, ChemPhysChem. 22 (2021) 1638–1644.

[33] K. Nagura, S. Saito, H. Yusa, H. Yamawaki, H. Fujihisa, H. Sato, Y. Shimoikeda, S. Yamaguchi, Distinct responses to mechanical grinding and hydrostatic pressure in luminescent chromism of tetrathiazolylthiophene, J. Am. Chem. Soc. 135 (2013) 10322–10325.

[34] M. Louis, C. Piñero García, A. Brosseau, C. Allain, R. Métivier, Mechanofluorochromism of a Difluoroboron-β-Diketonate Derivative at the Nanoscale, J. Phys. Chem. Lett. 10 (2019) 4758–4762.

[35] F.D. Lewis, J.-S. Yang, Solid-state fluorescence of aromatic dicarboxamides. Dependence upon crystal packing, J. Phys. Chem. B. 101 (1997) 1775–1781.

[36] C. Zheng, C. Zhong, C.J. Collison, F.C. Spano, Non-Kasha Behavior in Quadrupolar Dye Aggregates: The Red-Shifted H-Aggregate, J. Phys. Chem. C. 123 (2019) 3203–3215.

[37] G. Xia, Z. Jiang, S. Shen, K. Liang, Q. Shao, Z. Cong, H. Wang, Reversible specific vapoluminescence behavior in pure organic crystals through hydrogen-bonding docking strategy, Adv. Opt. Mater. 7 (2019) 1801549.

[38] K. Tanaka, Y. Chujo, Recent progress of optical functional nanomaterials based on organoboron complexes with β-diketonate, ketoiminate and diiminate, NPG Asia Materials. 7 (2015) e223.

[39] S. Corrent, P. Hahn, G. Pohlers, T.J. Connolly, J.C. Scaiano, V. Fornés, H. García, Intrazeolite Photochemistry. 22. Acid−Base Properties of Coumarin 6. Characterization in Solution, the Solid State, and Incorporated into Supramolecular Systems, J. Phys. Chem. B. 102 (1998) 5852–5858.

Highlights

1) New fluorescent molecule, **DFB-NH$_2$**, displays blue and blue-green luminescence in solution with QY > 90%.

2) Typical ICT nature was observed in the polar solvents, which is diminished upon protonation, reversibly.

3) Unique head-to-tail H-type dimer is displayed in the single crystal showing dark-red emission and mechanical smearing promoted blight yellow fluorescence as a blue-shifted mechanofuorochromism, MFC.

Journal Pre-proofs

4) Fluorescence color change with acid/base vapor was also reversibly observed in the polymer dispersed sample and even bulk crystalline powder samples.

Declaration of interests

☐ The authors declare that they have no known competing financial interests or personal relationships that could have appeared to influence the work reported in this paper.

☒ The authors declare the following financial interests/personal relationships which may be considered as potential competing interests:

TSUYOSHI KAWAI reports financial support was provided by Japan Society for the Promotion of Science. Clemence Allain reports financial support was provided by European Research Council. Marine Louis reports financial support was provided by NAIST Fundation. Shiho Katsumi reports financial support was provided by Japan Chemical Industry Association.

Journal Pre-proofs